Check for updates

Cu nanoparticles decorated WS$_2$ nanosheets as a lubricant additive for enhanced tribological performance

Zhuang Xu,[ab] Wenjing Lou, [ID][a] Gaiqing Zhao,[a] Dongdong Zheng,[a] Junying Hao[a] and Xiaobo Wang [ID] *[a]

Tungsten disulfide–polydopamine–copper (WS$_2$–PDA–Cu) nanocomposites were first prepared by a green and effective biomimetic strategy and then used as a lubricant additive in polyalkylene glycol (PAG). The biomimetic strategy is inspired by the adhesive proteins in mussels. WS$_2$ nanosheets were decorated by uniformly dispersed Cu nanoparticles (Cu NPs). The WS$_2$–PDA–Cu nanocomposites with good dispersion stability, showed better friction reducing and anti-wear properties than WS$_2$, Cu NPs and WS$_2$–Cu dispersed in PAG base oil. The average friction coefficient and wear volume were reduced by 33.56% and 97.95%, respectively, at 150 °C under a load of 100 N for the optimal concentration of 0.9 wt%. The lubrication mechanism was discussed.

1 Introduction

Friction and wear lead to a large energy loss and different types of equipment failure. The application of lubricants is one of the most important strategies for energy conservation and the reduction of friction and wear.[1–3] Lubricant additives play a vital role in improving the field service performance of base oil and in extending its service lifetime.[4,5] Anti-wear and friction reduction additives are common lubricant additives that are widely used in lubricating oil.[6] Since the invention of graphene, two-dimensional nanomaterials have been the focus of intense research due to their extraordinary physical and mechanical properties and have shown immense potential for use in a wide range of applications, particularly in lubricants.[7]

WS$_2$ is a two-dimensional nanomaterial that is a traditional solid lubricant additive due to its layered lattice structure. Zhang *et al.* investigated the tribological performance of WS$_2$ nanosheets as an additive in polyalpha olefin and gel lubricants. It was found that WS$_2$ nanosheets exhibit excellent friction reduction and anti-wear performance.[8] Jiang *et al.* prepared ultrathin WS$_2$ nanosheets and investigated the tribological properties of the nanosheets at different temperatures in poly-alpha olefin, thereby demonstrating that these nanosheets are highly effective for improving the friction reduction and anti-wear performance of base oil.[9] Zhang *et al.* prepared WS$_2$/TiO$_2$ nanoparticles successfully and studied their tribological performances, the results demonstrated that WS$_2$/TiO$_2$

remarkably improved the wear resistance of diisooctyl sebacate due to the synergistic lubrication effect of WS$_2$ and TiO$_2$.[10]

In addition to two-dimensional nanomaterials, metal nanoparticles, such as Cu NPs, Fe NPs, and Ag NPs, are another type of lubricant additives that are widely used in lubricating oils.[11,12] Cu NPs have attracted increasing attention for use as lubricant additives because of their low cost, environmental friendliness and high lubrication efficiency.[13] Xiong *et al.* reported oil-soluble Cu NPs and investigated their lubrication performance. The synthesized Cu NPs as an environmentally friendly additive in liquid paraffin showed excellent tribological performance characteristics for steel–steel contact.[14] Tarasov *et al.* prepared copper nanoparticles using an electrical explosion method and utilized these nanoparticles in motor oil. They explained the friction reduction properties of Cu NPs.[15] Yu *et al.* reported the tribological properties of Cu NPs in SN 650 oil and demonstrated the excellent friction reduction and anti-wear properties due to the formation of a thin copper film on the rough steel surface.[16] Moreover, few studies of the synergistic effect of Cu NPs and WS$_2$ mixture in solid lubrication have also been performed, showing excellent friction reduction and anti-wear properties.[17,18] Therefore, we have sufficient reason to conclude that Cu NPs uniformly decorated on WS$_2$ has a good synergistic effect in liquid lubricants. However, there is a significant lack of knowledge of the tribological performance characteristics of the uniformly decorated Cu NPs on WS$_2$ in liquid lubricants.

To demonstrate this concept, we first prepared WS$_2$–PDA–Cu nanocomposites by a green and effective biomimetic strategy and used the obtained nanocomposites as a lubricant additive in PAG. Our biomimetic strategy was inspired by the adhesive proteins in mussels and has been recently used as an efficient

[a]State Key Laboratory of Solid Lubrication, Lanzhou Institute of Chemical Physics, Chinese Academy of Sciences, Lanzhou 730000, China. E-mail: wangxb@licp.cas.cn
[b]University of Chinese Academy of Sciences, Beijing 100049, PR China

This journal is © The Royal Society of Chemistry 2019

surface modification technique.[19] PAG is important synthetic lubricating oil. PAG based lubricants have been used in many industrial applications for many years. The tribological performance of the WS_2–PDA–Cu nanocomposites used as an additive was investigated at an elevated temperature in PAG. The lubrication mechanism was discussed.

2 Materials and methods

2.1 Materials

WS_2 nanosheets were obtained from Beijing Dk Nano Technology Co., Ltd. (Beijing, China). Dopamine hydrochloride (DA, 98%) and tris-hydroxymethylaminomethane (tris, >99.9%) were purchased from Aladdin (Shanghai, China). $Cu(CH_3COO)_2 \cdot H_2O$ (precursor of Cu NPs) and $NaH_2PO_2 \cdot H_2O$ (reducing agent) were purchased from Macklin Biochemical Co., Ltd. (Shanghai, China). Polyalkylene glycol (PAG) was kindly provided by Weier Chemical Corporation (Nanjing, China). The typical technical value of the PAG oil are as follows: density is about 1.06 g cm^{-3} at 20 °C, acid value is 0.05 mg KOH per g, kinematic viscosity is 147.62 mm^2 s^{-1} at 40 °C, viscosity index is 210, and the flash point is 220 °C. All of the used chemical reagents were of analytical grade and were used as provided.

2.2 Synthesis of WS_2–PDA–Cu

The synthesized method of WS_2–PDA–Cu was the same as in the previous work, with some modifications.[13,20] The WS_2–PDA was synthesized *via* mussel-inspired chemistry. As shown in Scheme 1. In detail, 0.3 g WS_2 was dispersed in 100 mL tris buffer solution (pH = 8.5) and formed a homogeneous suspension. Then, 0.9 g DA was added and stirred for 8 h at room temperature. The product was collected by centrifuging at 6000 rpm for 10 min and was then washed several times with distilled water to remove the unreacted dopamine. The product was dried at 60 °C for 5 h in a vacuum oven.

Second, 0.05 g WS_2–PDA was dispersed in 200 mL ethanol by ultrasonication, and 0.375 g $Cu(CH_3COO)_2 \cdot H_2O$ was added into the solution under drastic stirring. After stirring for 1 h, the mixture was allowed to stand for 12 h. At this time, the upper layer of mixture was a bluish supernatant, and the WS_2–PDA was completely precipitated at the bottom. The bluish supernatant was poured out, and 200 mL ethanol was added into the precipitate. The mixture was ultrasonicated to again form a homogeneous solution. The solution was transferred into a three-necked flask (500 mL) fitted with a thermometer, a stirrer,
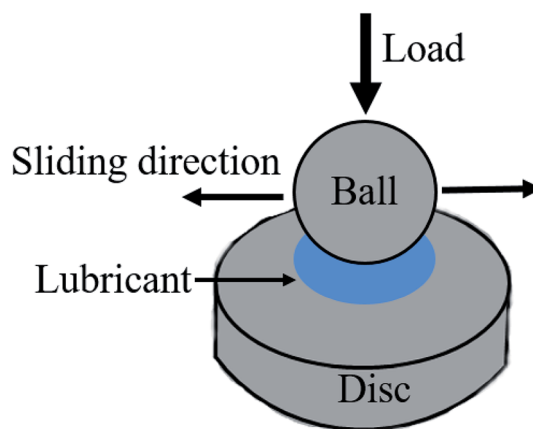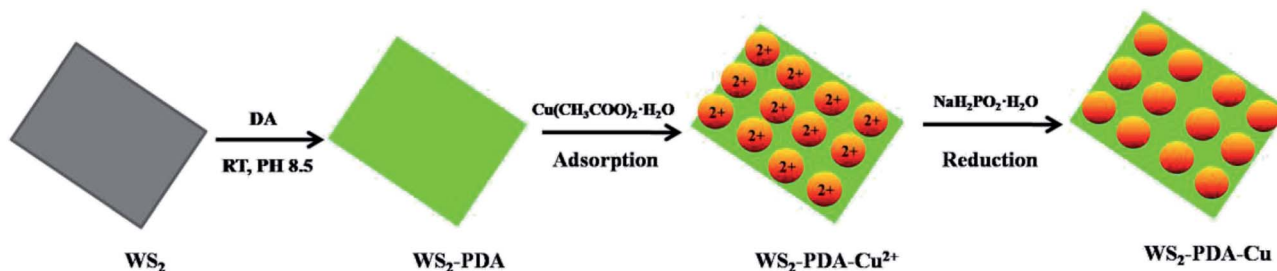

Scheme 2 Schematic of SRV-IV.

and a reflux condenser. $NaH_2PO_2 \cdot H_2O$ dissolved in 100 mL ethanol was added into the solution under vigorous stirring. The reaction process was maintained at 80 °C for 30 min. The solution was cooled down to room temperature and centrifuged under 7000 rpm for 10 min. The product was washed with ethanol several times to remove the remaining impurities. Finally, the prepared WS_2–PDA–Cu was dried by vacuum freeze-drying. The composites of WS_2–Cu were prepared in the same method without PDA. Cu NPs were prepared using the precursor and reducing agent under the same reaction conditions.

2.3 Characterizations and measurements

Fourier transform infrared (FTIR) spectra of WS_2–PDA–Cu were collected using a Bruker Tensor 27 FT-IR spectrometer. The surface morphology and microstructures of WS_2–PDA–Cu were observed using a JEOL TEM-2100 Plus high-resolution transmission electron microscope (HRTEM). Thermogravimetric analysis (TGA) was carried out using a thermogravimetric analyzer (Netzsch Sta 449 F5), ramping from 30 °C to 700 °C with a heating rate of 10 °C min^{-1} under nitrogen. The tribological properties were studied using the ball-on-disk apparatus of an Optimal SRV-IV oscillating reciprocating tester. Steel balls (∅ 10 mm, AISI 52100 bearing steel, hardness of 700 HV, R_a = 25 nm) and steel discs (∅ 24.00 × 7.88 mm, AISI 52100 bearing steel, hardness of approximately 625 HV, R_a = 48 nm) were used as frictional pairs in the tests (Scheme 2). The amount of lubricant of each test was approximately 0.5 mL. Repeating each test at least twice to minimize errors. The wear volume, cross-sectional

Scheme 1 Schematic of synthetic WS_2–PDA–Cu.

profile curve and morphology of the wear scars on the discs were measured using a MicroXAM-3D surface mapping profilometer and a scanning electron microscope (SEM, MERLIN compact 62-24), respectively. The chemical compositions of the WS_2–PDA–Cu and the wear scar surfaces were analyzed using an ESCALAB 250Xi X-ray photoelectron spectrometer (XPS).

3 Results and discussion

3.1 FT-IR spectra and thermal properties of WS_2–PDA–Cu

FTIR spectra of WS_2, WS_2–PDA and WS_2–PDA–Cu were investigated to confirm their chemical structures. The spectra are shown in Fig. 1. In contrast to WS_2 spectra, for the spectra of WS_2–PDA–Cu, the strong and broad band at approximately 3300 cm^{-1} is attributed to O–H/N–H of PDA.[21,22] The weak peak at 1760 cm^{-1} can be attributed to the C=O stretching vibration from dopamine derivatives. A new peak at 1650 cm^{-1} is attributed to the C=C stretching vibration of PDA. Another two peaks at 1560 cm^{-1} and 1338 cm^{-1} were observed, which can be attributed to the shearing vibration of N–H and formation vibration of C–H, respectively.[20] Moreover, WS_2–PDA spectra are similar to WS_2–PDA–Cu, indicating that the functional groups of PDA were still retained after the Cu NPs decorated the surfaces of WS_2–PDA. Additionally, this also demonstrates that WS_2 was successfully modified by PDA.

TGA was employed to provide insight into the thermal decomposition behavior of the grafted PDA molecules and decorated Cu NPs. Fig. 2 shows the TGA curves of WS_2, WS_2–PDA and WS_2–PDA–Cu. The weight loss of the pristine WS_2 nanosheets was 1.96%, which can be attributed to the absorbed impurities. After modification by PDA, the weight loss of WS_2–PDA was 23.1%. This shows that WS_2 has been modified with PDA. Moreover, the weight loss of WS_2–PDA–Cu was 9.54%. The weight loss of WS_2–PDA–Cu decreased significantly compared to that of WS_2–PDA, which may be ascribed to the decorated Cu NPs of WS_2–PDA.

3.2 Chemical composition and morphology of WS_2–PDA–Cu

The elements' chemical states and the composition of WS_2–PDA–Cu were investigated by XPS. Fig. 3 shows the high-
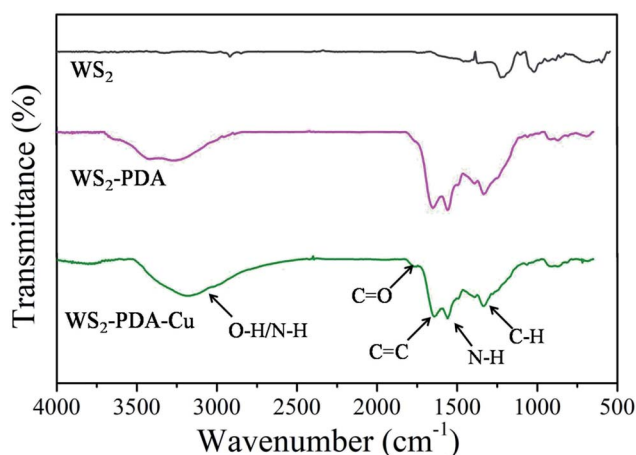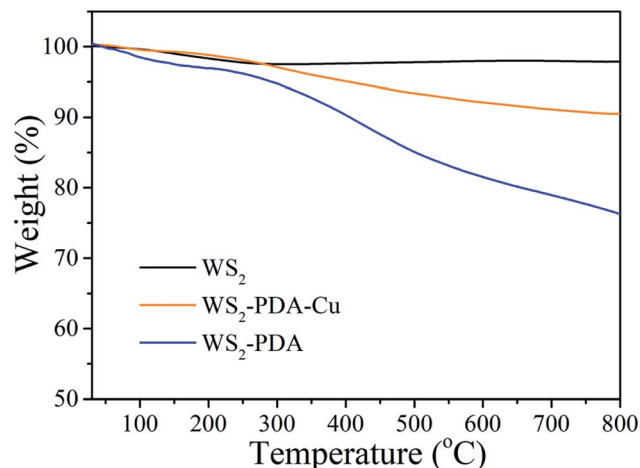

Fig. 2 TGA thermograms of WS_2, WS_2–PDA and WS_2–PDA–Cu.

resolution W 4f, S 2p, N 1s and Cu 2p XPS spectra of WS_2–PDA–Cu. The peaks of W 4f5/2 and W 4f7/2 at 34.8 eV and 32.5 eV correspond to the W–S bond. Two S 2p peaks are observed in the XPS spectrum at 163.3 eV and 162.2 eV that are ascribed to the S 2p1/2 and S 2p3/2 states of the S–W bond, respectively.[23] It was concluded that the W and S signals are due to the WS_2 nanosheets. The appearance of the N signal in WS_2–PDA–Cu is likely due to the grafted PDA. The peaks at approximately 401.5 eV and 399.9 eV attributed to C–NH_2 and C–NH, respectively, were observed.[24] The decoration of Cu NPs gives rise to the detection of Cu 2p1/2 and Cu 2p3/2 at the binding energies of approximately 952.6 eV and 933 eV,[11] respectively, which originated from WS_2–PDA–Cu. Therefore, these results further demonstrate that WS_2 was successfully modified by PDA and Cu NPs.

Fig. 4 shows the surface morphology of WS_2, WS_2–PDA, Cu NPs, WS_2–Cu and WS_2–PDA–Cu. A new organic layer is clearly observed at the edge of WS_2–PDA, as seen in Fig. 4a and b. This indicated that WS_2 was successfully modified with PDA. Fig. 4c shows the spherical Cu NPs. The micro morphology of WS_2–Cu shows that Cu NPs with a diameter of approximately 100 nm are randomly dispersed on the WS_2 nanosheets (Fig. 4d). By contrast, as shown in Fig. 4e, Cu NPs are evenly dispersed on WS_2–PDA nanosheets. Moreover, the diameter of Cu NPs is observed to be in the range of 10–20 nm. Fig. 4f shows the magnified TEM image of WS_2–PDA–Cu, and a crystal lattice spacing of 0.21 nm was observed which in agreement with the (111) plane spacing of crystalline Cu.[25] To summarize, WS_2 was successfully modified by PDA and Cu was subsequently uniformly anchored on the WS_2–PDA surface.

The dispersion stability of the WS_2–PDA–Cu and WS_2–Cu in base oil was investigated by digital images. As shown in Fig. 5, the dispersed WS_2–Cu in the base oil gradually precipitated with the increasing time and a large amount of sediment appeared after 7 days. By contrast, a stable dispersion of WS_2–PDA–Cu was found. This finding shows that the dispersion stability of the WS_2–PDA–Cu is due to Cu NPs preventing WS_2 from restacking, as well as to the functional –OH and –NH groups contributing to the dispersion in the polar PAG base oil.
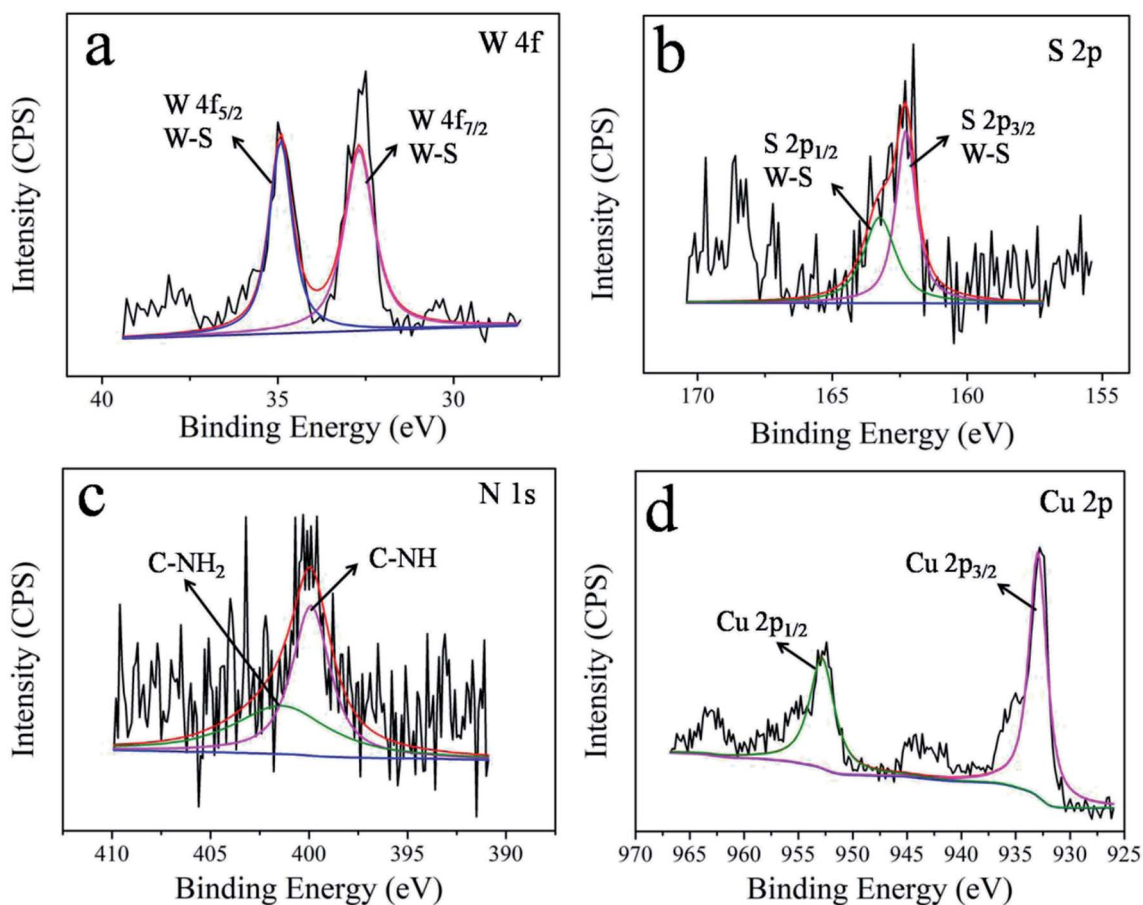

Fig. 1 The FTIR spectra of WS_2, WS_2–PDA and WS_2–PDA–Cu.

Fig. 3 High-resolution XPS spectra of W (a), S (b), N (c) and Cu (d) regions for WS_2–PDA–Cu.

3.3 Tribological properties of WS_2–PDA–Cu

The tribological performances of various nanomaterials used as additives in PAG were studied for steel/steel contact at 150 °C. As shown in Fig. 6a, compared with the base oil, the friction coefficients of the dispersed lubricant filled with various nanomaterials was lower. This result demonstrates that all studied nanomaterials have good friction reduction properties. Compared with base oil, the friction coefficient mean value of WS_2, Cu, WS_2–Cu and WS_2–PDA–Cu was reduced by 15.4%, 11.41%, 13.42% and 33.56%, respectively. Clearly, the friction coefficient of 0.9 wt% WS_2–PDA–Cu nanocomposites was the
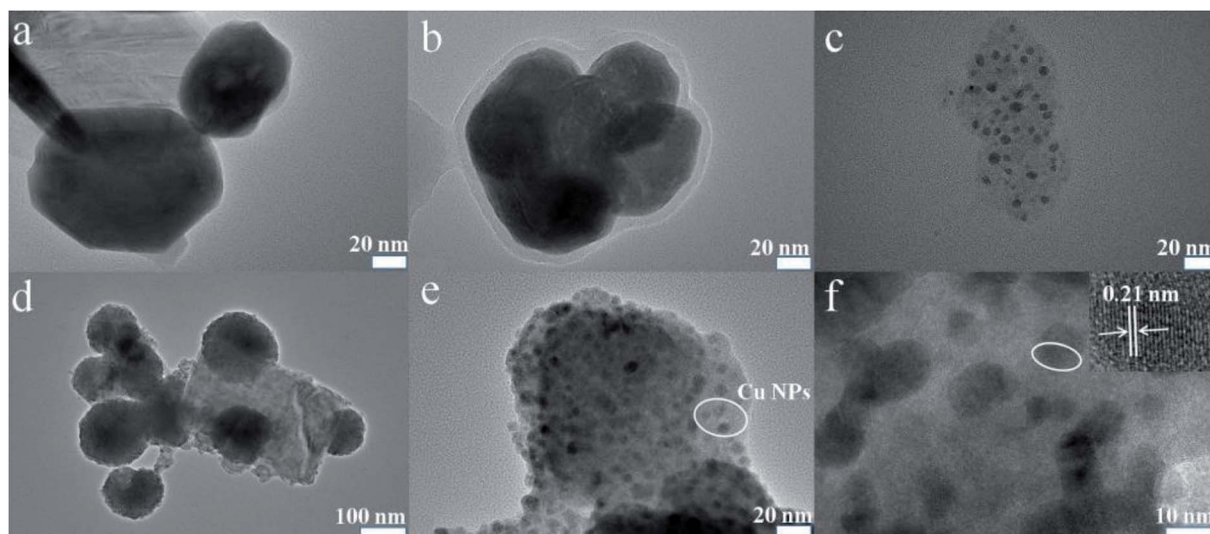

Fig. 4 TEM images of WS_2 (a), WS_2–PDA (b), Cu NPs (c), WS_2–Cu (d) and WS_2–PDA–Cu (e and f).
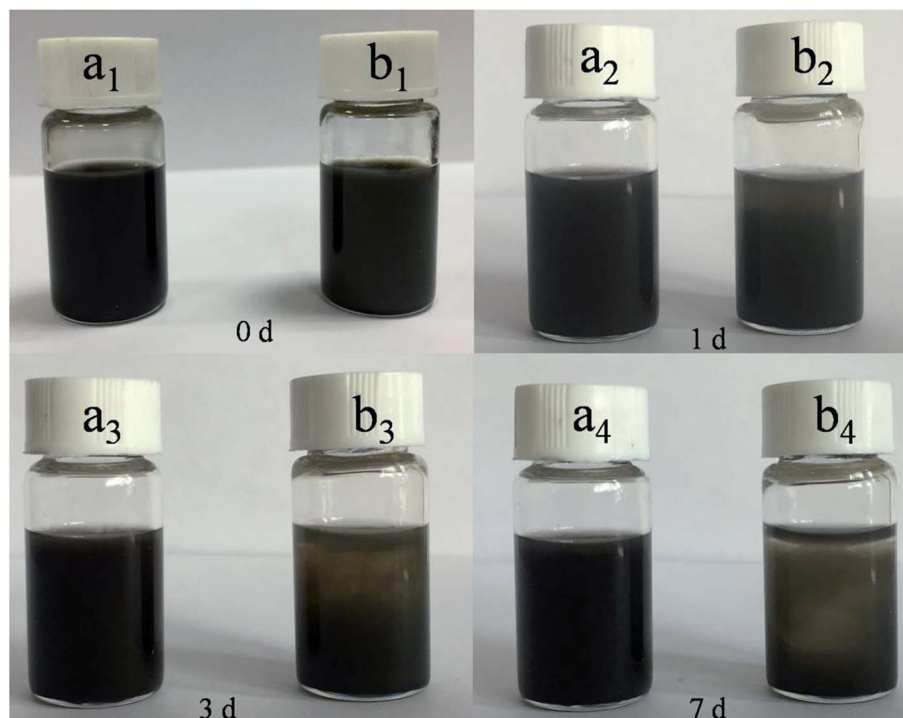
Fig. 5 Dispersion of WS$_2$–PDA–Cu (a$_1$–a$_4$) and WS$_2$–Cu (b$_1$–b$_4$) in PAG base oil.

lowest, displaying the optimal friction reduction performance. The wear volume values of the discs lubricated by base oil and base oil containing different additives are shown in Fig. 6b. It is clearly observed that the wear volume of the dispersed lubricants filled with various nanomaterials decreased significantly. In detail, the wear volume values of WS$_2$, Cu, WS$_2$–Cu, WS$_2$–PDA–Cu decreased by 76.54%, 59.40%, 64.80% and 97.95%, respectively, relative to that of base oil. This result established that WS$_2$–PDA–Cu nanocomposites also have the optimal anti-wear property. Therefore, the adding of reference nano-materials can improve the tribological performances of base oil. In particular, WS$_2$–PDA–Cu provides the most effective

improvement of the tribological performance characteristics of base oil.

Fig. 7 shows the friction coefficient and wear volume of the dispersed lubricants containing various concentrations of WS$_2$–PDA–Cu. An examination of Fig. 7a shows that the friction coefficient decreases with increasing concentration of WS$_2$–PDA–Cu. The lowest friction coefficient was obtained at the WS$_2$–PDA–Cu concentration of 0.9 wt%. However, higher friction was observed with increasing concentration of WS$_2$–PDA–Cu. As shown in Fig. 7b, as the concentration increases, wear volume become gradually lower than that of base oil until the lowest value is obtained at the concentration of 0.9 wt%.
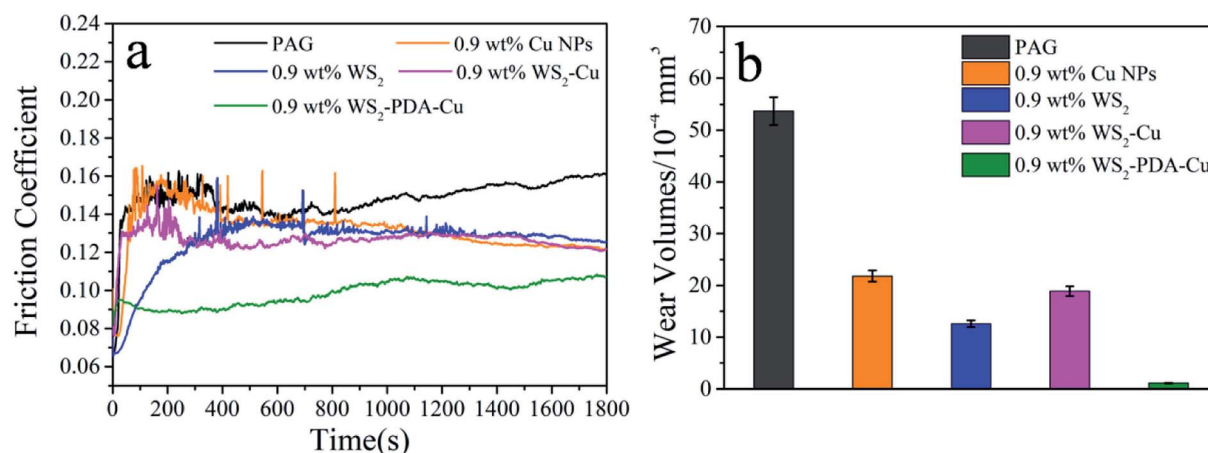

Fig. 6 Friction coefficient (a) and wear volume (b) of the discs lubricated by PAG containing different additives (load, 100 N; temperature, 150 °C; stroke, 1 mm; frequency, 25 Hz).
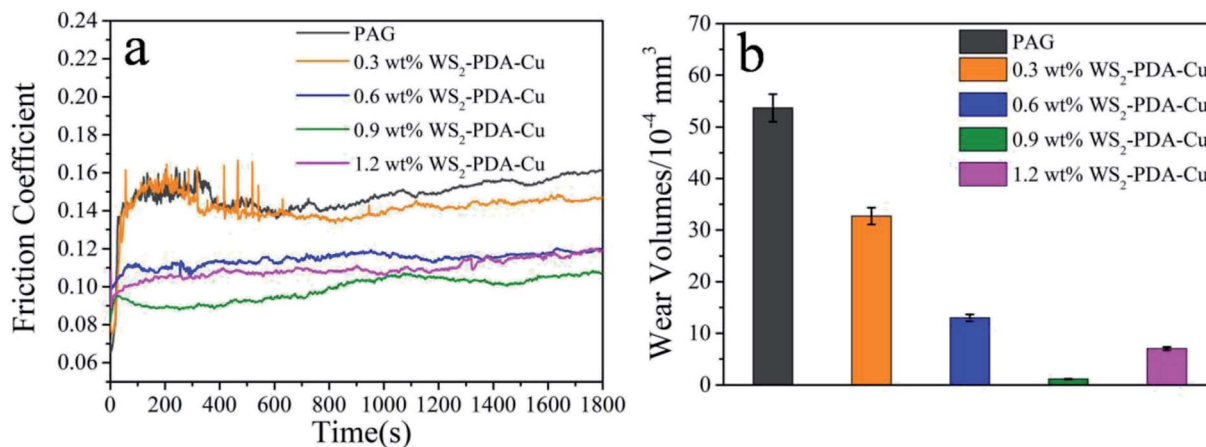
Fig. 7 Friction coefficient (a) and wear volume (b) of the discs lubricated by PAG containing WS$_2$–PDA–Cu with different concentrations (load, 100 N; temperature, 150 °C; stroke, 1 mm; frequency, 25 Hz).
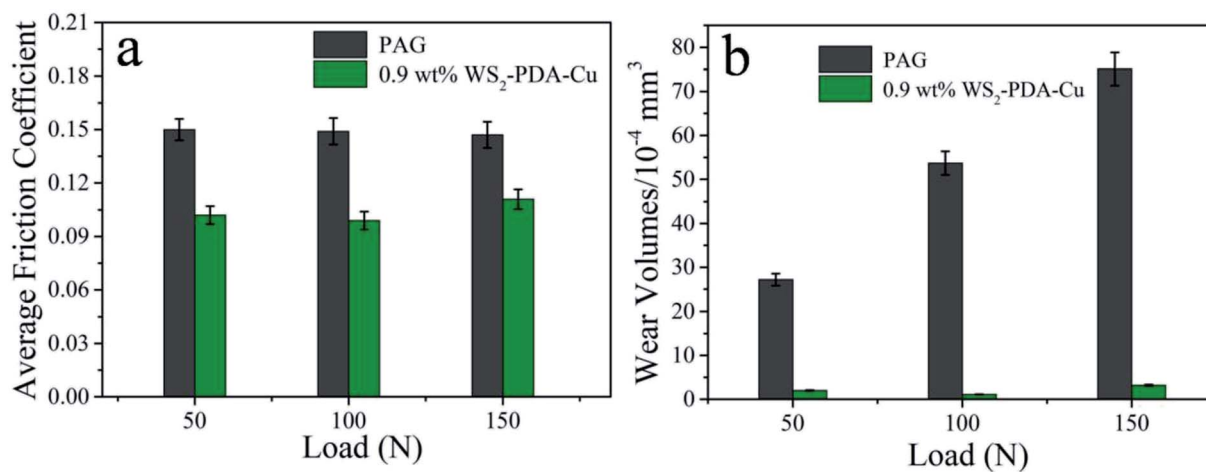

Fig. 8 Average friction coefficient and wear volume of the discs lubricated by PAG and PAG containing 0.9 wt% WS$_2$–PDA–Cu under various loads (temperature, 150 °C; stroke, 1 mm; frequency, 25 Hz).
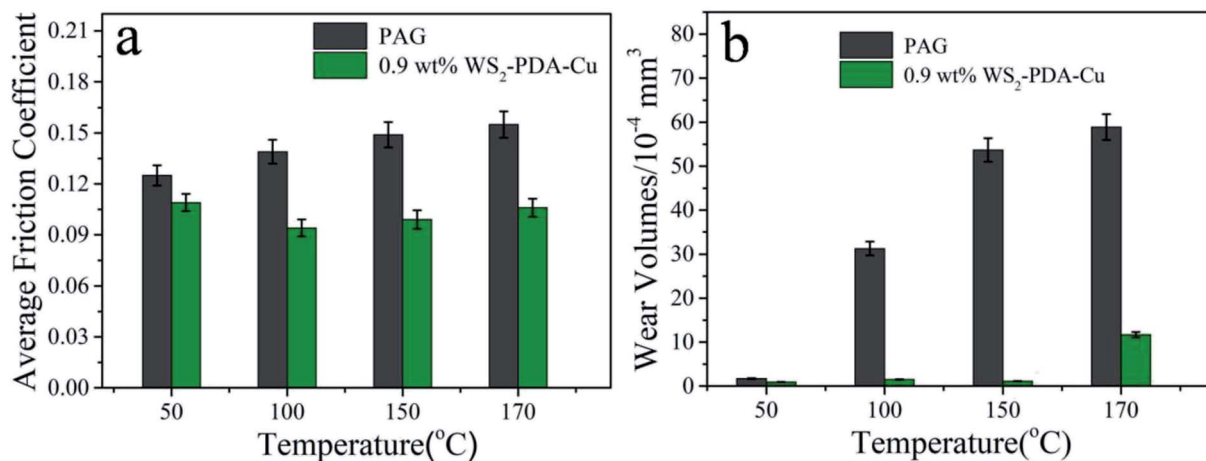

Fig. 9 Average friction coefficient and wear volume of the discs lubricated by PAG and PAG containing 0.9 wt% WS$_2$–PDA–Cu at various temperature (load, 100 N; stroke, 1 mm; frequency, 25 Hz).

Nevertheless, when the concentration increased to 1.2 wt%, the wear volume was slightly higher than that at the concentration of 0.9 wt%. Therefore, these results reveal that the optimal concentration is 0.9 wt%, giving the best lubricating performance for the base oil. It is plausible that the higher concentration of WS₂–PDA–Cu between the contact interfaces of the frictional pairs leads to an abrasive effect that increases friction and wear.[7]

The tribological performances of base oil and base oil containing 0.9 wt% WS₂–PDA–Cu under various loads were studied, as shown in Fig. 8. It is clear that WS₂–PDA–Cu displays excellent lubricating performance under different loads in base oil. The average friction coefficient exhibits similar variation trend to that of the wear volume. The average friction coefficient and wear volume are reduced by 33.56% and 97.95%, respectively,

under the load of 100 N, followed by 32.0% and 92.65%, respectively, under 50 N, and 24.49% and 95.74%, respectively, under 150 N. Moreover, the wear volume of base oil containing 0.9 wt% WS₂–PDA–Cu is slightly higher than 100 N under 50 N loads. This may be due to the fact that the temperature played an active role in improving the tribological behavior of base oil in the presence of additives. The friction pair forms a lower instantaneous temperature at 50 N loads compared to the 100 N loads, which does not promote the tribo-chemical reaction to form a sufficient lubricating film. Taken together, these results demonstrated that the optimal friction reduction and anti-wear performance appears under the load of 100 N.

As shown in Fig. 9, the friction reduction and anti-wear properties of base oil and base oil with 0.9 wt% WS₂–PDA–Cu were further investigated at various temperatures under
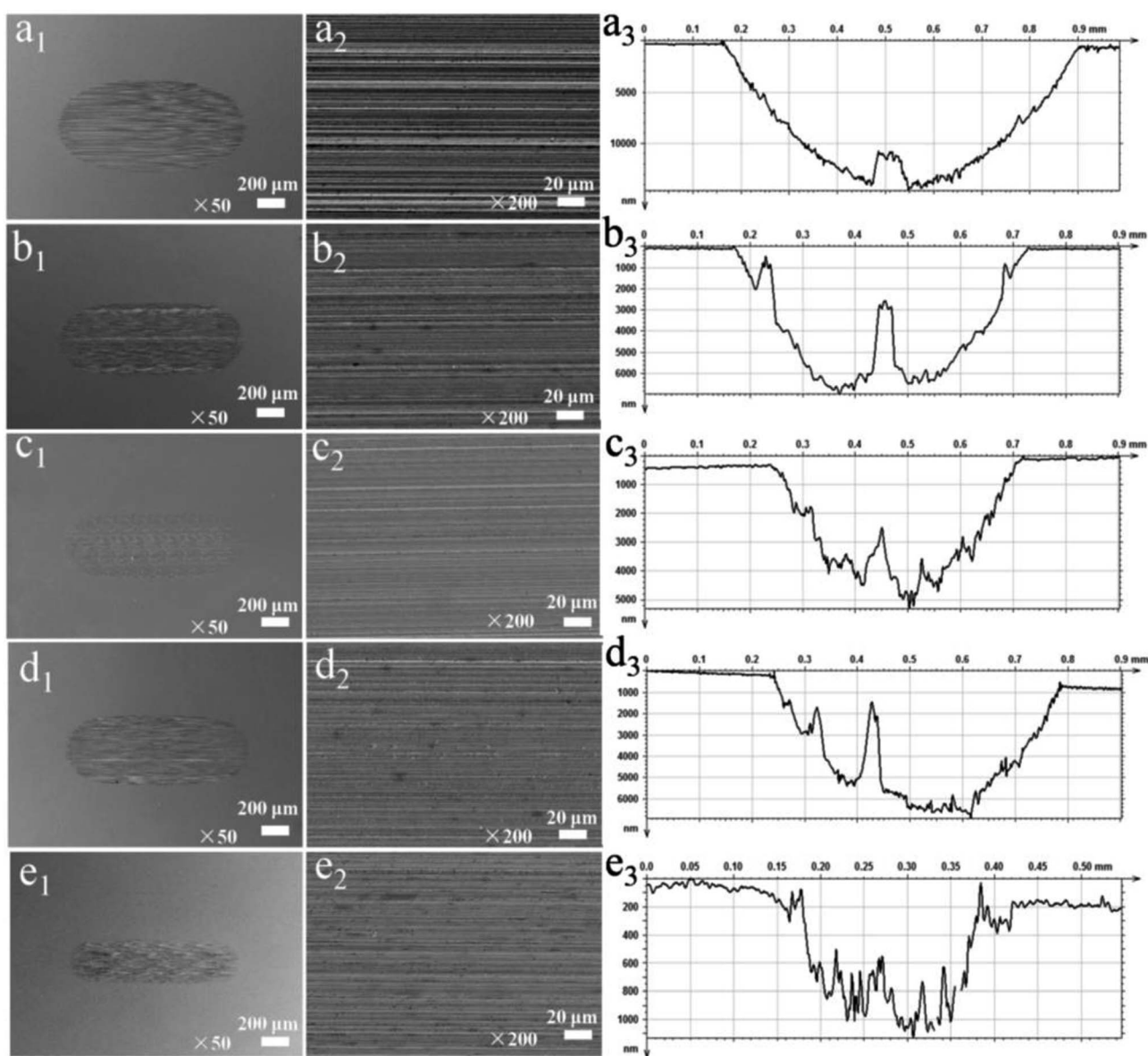

Fig. 10 SEM images and cross-sectional profile curve of the worn scar lubricated by base oil and base oil containing different additives (load, 100 N; temperature, 150 °C; stroke, 1 mm; frequency, 25 Hz): (a₁–a₃) base oil; (b₁–b₃) 0.9 wt% Cu NPs; (c₁–c₃) 0.9 wt% WS₂; (d₁–d₃) 0.9 wt% WS₂–Cu and (e₁–e₃) 0.9 wt% WS₂–PDA–Cu.

a constant load of 100 N. It was observed noted that the average friction coefficient and wear volume of WS$_2$–PDA–Cu decreased more strongly relative to base oil as the temperature increased in the 50–170 °C range. The average friction coefficient and wear volume were reduced by 33.56% and 97.95%, respectively, at 150 °C, by 12.8% and 47.06%, respectively, at 50 °C, by 32.37% and 95.21%, respectively, at 100 °C, and by 31.61% and 80.14% at 170 °C. At a higher temperature, thermal activation may promote the chemical reaction between WS$_2$–PDA–Cu and the interfaces, which is more conducive to the formation of the lubricating film. The application of WS$_2$–PDA–Cu in base oil may form a lubricating film that maintains lower friction and wear when the temperature is increased.[26] Moreover, when the temperature reaches 170 °C, since the additive is decomposed in a small amount at a high temperature, the formed lubricating film cannot be quickly replenished to cause a slightly increase in wear.

To further elucidate the impact of different additives on the anti-wear performance, the surface morphologies and cross-sectional profile curve of the wear scars of different dispersed lubricants were observed. Fig. 10(a$_1$–a$_3$) shows that the discs lubricated by base oil exhibit larger and deeper wear scars with scratches and grooves, indicating that severe wear was experienced by the surface. A more narrow and much more shallow wear scars were observed on the discs lubricated by the base oil containing the additives. Moreover, the wear scar lubricated by base oil with 0.9 wt% WS$_2$–PDA–Cu was the narrowest and shallowest compared to the other additives (e$_1$–e$_3$). This result is in agreement with the values of the wear volume presented in Fig. 6b. Therefore, WS$_2$–PDA–Cu can impart excellent anti-wear properties to the base oil.

The identification of the chemical states of the elements of the wear surface is a useful approach that provides strong indication for the lubrication mechanism of WS$_2$–PDA–Cu that gives rise to the improved tribological properties. The XPS spectra of Fe 2p, W 4f, S 2p and Cu 2p are shown in Fig. 11. Two peaks of Fe 2p at 710.6 eV and 724.9 eV were detected that are ascribed to FeS$_2$, FeO, Fe$_2$O$_3$, FeOOH, and Fe$_3$O$_4$.[27] The W 4f XPS spectrum contained two peaks at 35.05 eV and 37.2 eV that were attributed to W 4f5/2 and W 4f7/2, respectively, corresponding to WS$_2$ and WO$_3$.[23] The S 2p peak appeared at 168.1 eV, corresponding to WS$_2$, FeSO$_4$ and Fe$_2$(SO$_4$)$_3$.[28] The Cu 2p spectrum peaks were located at 933.2 eV and 952.6 eV and were ascribed to the Cu 2p3/2 and Cu 2p1/2 signals, respectively.[29] These results demonstrate that WS$_2$–PDA–Cu in base oil leads to the formation of an adsorbed film and tribo-chemical film. At the initial stage of the sliding, the WS$_2$–PDA–Cu nanocomposites in base oil fill up the grooves of the rough surface of the friction
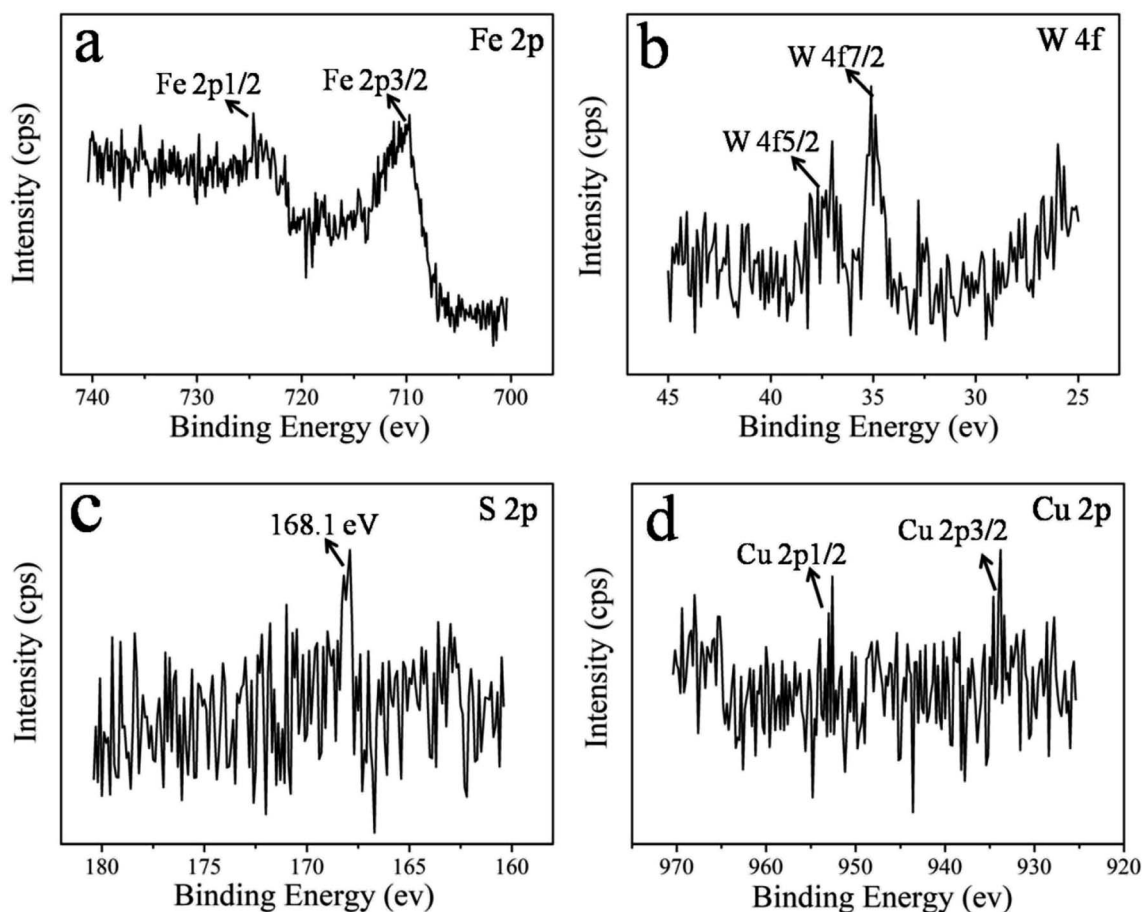

Fig. 11 XPS spectra of wear surfaces on the discs lubricated by PAG containing WS$_2$–PDA–Cu (load, 100 N; temperature, 150 °C; stroke, 1 mm; frequency, 25 Hz), Fe 2p (a), W 4f (b), S 2p (c) and Cu 2p (d).

pair due to physical adsorption, forming an adsorption film. The film maintains low friction and wear. With the progress of the sliding process, the tribo-chemical reaction will occur when the real contact pressure and the flash temperature match the reaction potential energy.[14] These two kinds of films can protect the friction pairs during the sliding process, and therefore play a friction reduction and anti-wear role, leading to better lubricating effects.

Cu NPs act as tiny bearings between the contact interfaces to prevent the direct contact of frictional pairs. The polar amines functional groups in WS_2–PDA–Cu are easily adsorbed to the friction interfaces, promoting the formation of the adsorption film and the tribo-chemical films. Moreover, the uniformly dispersed Cu NPs enhance the load carrying capacity of WS_2 nanosheets. In summary, these gave rise to the appearance of the significantly synergistic effect between Cu NPs and WS_2 nanosheets.[20,30]

4 Conclusions

We first prepared WS_2–PDA–Cu nanocomposites by a green and effective biomimetic strategy and used the obtained nanocomposites as a lubricant additive in PAG. WS_2 nanosheets were decorated by uniformly dispersed Cu NPs. The tribological performance of WS_2–PDA–Cu nanocomposites as an additive was investigated at an elevated temperature, showing better friction reduction and anti-wear properties compared with the PAG base oil and PAG containing WS_2, Cu NPs or WS_2–Cu. The average friction coefficient and wear volume was reduced by 33.56% and 97.95%, respectively, at 150 °C under a load of 100 N with the optimal WS_2–PDA–Cu concentration of 0.9 wt%. The WS_2–PDA–Cu in base oil leads to the formation of an adsorbed film and a tribo-chemical film, thereby reducing friction and wear. The present work demonstrates the potential application of WS_2–PDA–Cu as an effective additive for lubricants.

Conflicts of interest

There are no conflicts to declare.

Acknowledgements

References

1 R. A. E. Wright, K. W. Wang, J. Qu and B. Zhao, *Angew. Chem., Int. Ed.*, 2016, **55**, 1–6.
2 C. Greiner, Z. L. Liu, L. Strassberger and P. Gumbsch, *ACS Appl. Mater. Interfaces*, 2016, **8**, 15809–15819.
3 N. Salah, M. S. Abdel-wahab, A. Alshahrie, N. D. Alharbi and Z. H. Khan, *RSC Adv.*, 2017, **7**, 40295–40302.
4 G. Karmakar and P. Ghosh, *ACS Sustainable Chem. Eng.*, 2016, **4**, 775–781.
5 Y. G. Zhang, W. Z. Wang, H. Liang and Z. Q. Zhao, *Tribol. Int.*, 2019, **131**, 137–147.
6 G. Karmakar and P. Ghosh, *ACS Sustainable Chem. Eng.*, 2015, **3**, 19–25.
7 S. Kumari, O. P. Sharma, R. Gusain, H. P. Mungse, A. Kukrety, N. Kumar, H. Sugimura and O. P. Khatri, *ACS Appl. Mater. Interfaces*, 2015, **7**, 3708–3716.
8 R. C. Zhang, D. Qiao, X. Q. Liu, Z. G. Guo, M. R. Cai and L. Shi, *Tribol. Int.*, 2018, **118**, 60–70.
9 Z. Q. Jiang, Y. J. Zhang, G. B. Yang, K. P. Yang, S. M. Zhang, L. G. Yu and P. Y. Zhang, *Tribol. Lett.*, 2016, **61**, 24–38.
10 Z. Y. Lu, Z. Z. Cao, E. Z. Hu, K. H. Hu and X. G. Hu, *Tribol. Int.*, 2019, **130**, 308–316.
11 B. S. Zhang, B. S. Xu, Y. Xu, F. Gao, P. J. Shi and Y. X. Wu, *Tribol. Int.*, 2011, **44**, 878–886.
12 W. Dai, B. Kheireddin, H. Gao and H. Liang, *Tribol. Int.*, 2016, **102**, 88–98.
13 Z. Q. Wang, R. R. Ren, H. J. Song and X. H. Jia, *Appl. Surf. Sci.*, 2018, **428**, 630–639.
14 X. J. Xiong, Y. K. Kang, G. B. Yang, S. M. Zhang, L. G. Yu and P. Y. Zhang, *Tribol. Lett.*, 2012, **46**, 211–220.
15 S. Tarasov, A. Kolubaev, S. Belyaev, M. Lerner and F. Tepper, *Wear*, 2002, **252**, 63–69.
16 H. L. Yu, Y. Xu, P. J. Shi, B. S. Xu, X. L. Wang, Q. Liu and H. M. Wang, *Surf. Coat. Technol.*, 2008, **203**, 28–34.
17 J. K. Xiao, W. Zhang and C. Zhang, *Wear*, 2018, **412–413**, 109–119.
18 R. Tyagi, A. K. Das and A. Mandal, *Tribol. Int.*, 2018, **120**, 80–92.
19 J. H. Ryu, P. B. Messersmith and H. Lee, *ACS Appl. Mater. Interfaces*, 2018, **10**, 7523–7540.
20 H. J. Song, Z. Q. Wang, J. Yang, X. H. Jia and Z. Z. Zhang, *Chem. Eng. J.*, 2017, **324**, 51–62.
21 G. J. Zeng, M. Y. Liu, X. H. Liu, Q. Huang, D. Z. Xu, L. C. Mao, H. Y. Huang, F. J. Deng, X. Y. Zhang and Y. Wei, *Appl. Surf. Sci.*, 2016, **387**, 399–405.
22 Z. Xu, W. J. Lou, X. H. Wu, X. B. Wang and J. Y. Hao, *RSC Adv.*, 2017, **7**, 53346–53354.
23 P. U. Aldana, B. Vacher, T. L. Mogne, M. Belin, B. Thiebaut and F. Dassenoy, *Tribol. Lett.*, 2014, **56**, 249–258.
24 Z. X. Yu, F. Li, Q. B. Yang, H. Shi, Q. Chen and M. Xu, *ACS Sustainable Chem. Eng.*, 2017, **5**, 7840–7850.
25 Y. W. Tai, Y. C. Chiu, P. T. Wu, J. S. Yu and Y. C. Chin, *ACS Appl. Mater. Interfaces*, 2018, **10**, 5161–5174.
26 J. Zhao, Y. Y. He, Y. F. Wang, W. Wang, L. Yan and J. B. Luo, *Tribol. Int.*, 2016, **97**, 14–20.
27 X. H. Wu, G. Q. Zhao, Q. Zhao, K. L. Gong, X. B. Wang, W. M. Liu and W. S. Liu, *RSC Adv.*, 2016, **101**, 98606–98610.
28 V. Koroteev, L. Bulusheva, I. Asanov, E. Shlyakhova, D. Vyalikh and A. Okotrub, *J. Phys. Chem. C*, 2011, **115**, 21199–21204.
29 S. H. Al-Harthi, M. Al-Barwani, M. Elzain, A. T. Al-Hinai, N. Al-Naamani, I. Al-Amri and T. Hysen, *Appl. Phys. A: Mater. Sci. Process.*, 2011, **105**, 469–477.
30 H. X. Wu, L. G. Qin, G. N. Dong, M. Hua, S. C. Yang and J. F. Zhang, *Tribol. Int.*, 2017, **107**, 48–55.